Hitting probabilities of diffusion-limited-aggregation clusters

Marek Wolf
Institute of Theoretical Physics, University of Wroclaw, PL-50-205 Wroclaw, Cybulskiego 36, Poland
(Received 10 May 1990; revised manuscript received 26 November 1990)

A method of calculating growth probabilities of the diffusion-limited-aggregation (DLA) clusters is presented. This method is based on the Spitzer theorem and allows very accurate determination of the probabilities of hitting the random walkers by the perimeter of the cluster even deeply in the "fjords," where the probabilities are small. The multifractal spectrum $f(\alpha)$ is determined, and evidence for the phase transition is found. The large fluctuations of the minimal growth probabilities between different DLA clusters were found. A comparison of this method with the ones applied previously is also given.

I. INTRODUCTION

In the past decade there has been increasing interest in the study of irreversible kinetic processes leading to the formation of fractal objects. A simple stochastic model for the formation of clusters of particles in two-dimensional space was proposed by Witten and Sander.[1] In their model, called diffusion-limited aggregation (DLA), a single particle walks randomly on a square lattice until it reaches another particle ("seed") usually located in the center of the lattice. Then, a new particle initiates its random walk. If the particle contacts the cluster (now built of two particles), it is incorporated into the cluster and the cluster grows. This process is repeated many times ($\sim 10^3$–10^6) and leads to ramified structures possessing remarkable scaling properties. For example, the number N of particles contained inside a circle of radius R grows as

$$N(R)\sim R^D , \tag{1}$$

where $D\approx 1.7$ is the fractal dimension. Many modifications and different techniques for computer simulations have been discussed (for reviews see, e.g., Refs. 2–6). Besides this "computer phenomenology," a number of real experiments were also performed, such as electrodeposition,[7] electric breakdown in dielectrics,[8] fluid flows in porous media, and viscous fingers.[9]

To our knowledge there still does not exist a satisfactory theory of the general growth processes, and of DLA in particular. The basic ingredients of the whole theory should only be the coordinates of the aggregated particles—all other quantities should be expressed by them. Two different theoretical approaches can be distinguished. Initially, the attempts were concentrated on the analytical derivation of the scaling law (1) and of the fractal dimension D by means of the mean-field arguments[10,11] and real-space renormalization-group methods.[12,13] The breakthrough appeared with the recognition of the role played by the set of the growth probabilities $\{p_s\}_{s\in\Gamma}$, where p_s is the probability that the perimeter site s is the next to grow[14–16] and Γ is the set of the nodes on the perimeter of a given DLA cluster. The customary way of studying the properties of the set of probabilities $\{p_s\}$ is by means of the moments

$$Z_q(R)=\sum_s p_s^q , \tag{2}$$

where R is the linear size (radius of gyration) of the aggregate and $q\in\mathbb{R}$. In early works[15–19] the powerlike dependence of the moments on R was found:

$$Z_q(R)\sim R^{-\tau(q)} . \tag{3}$$

The fact that the function $\tau(q)$ is not linear is called multifractality[20,21] and the function $f(\alpha)$ obtained by means of the Legendre transform of $\tau(q)$ with respect to the variable q,

$$\alpha(q)=\frac{d\tau}{dq},\quad f(\alpha)=q\alpha(q)-\tau(q) , \tag{4}$$

is called the multifractal spectrum.

A new theoretical approach to DLA was proposed by Pietronero *et al.*[22] which aimed at the calculation of both the fractal dimension D and the multifractal spectrum $f(\alpha)$. In a series of recent papers[23–28] the problem of the phase transition in the multifractal spectrum of diffusion-limited aggregation was discussed. In particular, the authors of Refs. 23 and 25 have performed the extensive enumeration of *all* DLA clusters in the square lattices of up to 5×5 sites and they found the breakdown of the scaling law at $q_c=-1$. The word "all" means that the moments (2) were averaged over *all* possible clusters of a given size. In such a way Stanley *et al.* were able to account for very rare configuration with extremely small p_s. This caused an increase of the moments for negative q. Next, Blumenfeld and Aharony[24] (BA), assuming the exponential decreasing of the minimal probability $p_{\min}$ with the size of the aggregate for *typical* configuration, also gave analytical arguments for the existence of the phase transition for the moments of a single cluster [as in Eq. (2), i.e., without averaging]. BA have made the claim that, besides q_c, there should also exist a second characteristic value of q, q_0, at which the functions $f(q)$ and $\alpha(q)$ become independent of q. The first evidence of

the phase transition for a *single typical* cluster appeared earlier in Ref. 27.

The detection of the phase transition is a problem of the numerical nature—the breakdown of the mutlifractality is linked to the sites with very small hitting probabilities, and to get reliable results, the accuracy of the calculation of p_s's should be many orders smaller than $p_{\min}$. In early papers[15,17] the growth probabilities were estimated by successive launching of a lot (10^5–10^6) of walkers and recording of the point of first contact with a cluster. It is obvious that such a number of walkers does not allow an accurate estimation of the probabilities deep inside the fjords, where $p_s < 10^{-6}$. Next, the method based on the analogy between dielectric breakdown model (DBM) and DLA (Ref. 8) and consisting in solving Laplace's equation on the lattice was used very often.[19,22,27] In this paper I am going to present another method of calculation of the growth probabilities which possesses the advantage of high accuracy. This method is based on Spitzer's theorem[29] and probably in some sense is equivalent to the methods used in Refs. 14 and 16. It allows very accurate determination of the growth probabilities—for the completely screened sites, instead of $p_s=0$, I have at times obtained p_s of the order of 10^{-20} (see Table II and Fig. 17). While DLA clusters are not large, this method provides information on the occupancy probabilities, which in the usual technique of brute-force Monte Carlo simulation or solving the Laplace equation can only be achieved by many realizations or iterations at each stage of the growth.

In Sec. II, I present the theorem of Spitzer, allowing the calculation of the hitting probabilities of the random walk by arbitrary sets. In Sec. III the implementation of the method is described and Sec. IV is devoted to discussion of the "static" scaling laws between the radius, the number of particles, and the number of perimeter sites. The problem of whether the scaling (3) holds for negative q is treated in Sec. V. It is found that in fact for the *typical* clusters the breaking of (3) is not significant and the function $f(\alpha)$ can be determined. In Sec. VI the "local" multifractality introduced in Refs. 23–26 is discussed. In Sec. VII the way of decay of the minimum growth probability of typical DLA configuration is discussed. Unfortunately, the sizes of the clusters are not sufficiently large for a firm conclusion of the question, is the decay of the typical minimum growth probability exponential or powerlike. In Sec. VIII a comparison with other methods is presented and Sec. IX contains a summary of the results.

II. THE HITTING PROBABILITIES OF THE FINITE SET

Usually, the DLA cluster is grown by successive accretion of random walkers to perimeter sites or the analogy with DBM (see Sec. VIII) is used. In this paper, however, I shall use the Spitzer formula[29] expressing the hitting probabilities of an arbitrary finite set for the arbitrary aperiodic recurrent random walk in two dimensions.

Because in the usual DLA the particles perform the symmetric random walk in a two-dimensional lattice $\mathbb{Z}_2$, I will describe here the Spitzer recipe for calculating the hitting probabilities of a *simple* random walk by points belonging to a finite set B containing at least two sites. For the simple random walk the transition probability $P(x,y)$ is of the form

$$P(x,y)=\begin{cases}\frac{1}{4} & \text{if } x \text{ and } y \text{ are nearest-neighbor sites}\\ 0 & \text{in other cases.}\end{cases} \tag{5}$$

As is well known, this random walk is symmetric aperiodic, and recurrent (recall that in more than two dimensions the symmetric random walk is not recurrent, i.e., the probability of a walker hitting the given fixed point is less than 1). Let $P_n(x,y)$ denote the probability that a particle executing a random walk and starting at the point x will reach the point y after n steps:

$$P_n(x,y)=\sum_{x_i\in\mathbb{Z}_2,\, i=1,\ldots,n-1} P(x,x_1)P(x_1,x_2)\cdots P(x_{n-1},y)\ . \tag{6}$$

Let $G_n(x,y)$ denote the expected number of visits of the random walk starting at x to the point y within n steps:

$$G_n(x,y)=\sum_{k=1}^{n} P_k(x,y)\ . \tag{7}$$

The crucial quantity in the Spitzer formula is the potential kernel defined as

$$A_n(x,y)=G_n(0,0)-G_n(x,y)\ . \tag{8}$$

Let $A(x,y)$ denote the limit

$$A(x,y)=\lim_{n\to\infty} A_n(x,y)\ . \tag{9}$$

It can be proved that the operator $A(x,y)$ is symmetric and, if restricted to any finite subset B of $\mathbb{Z}_2$, invertible; let $K_B(x,y)$ denote this inverse matrix:

$$\sum_{t\in B} A(x,t)K_B(t,y)=\delta(x,y) \quad \text{for } x,y\in B\ . \tag{10}$$

Next let us introduce the notation

$$K_B(x)=\sum_{t\in B} K_B(x,t)\ , \tag{11a}$$

$$K_B=\sum_{t\in B} K_B(t)\ . \tag{11b}$$

Let $H_B(x,y)$ denote the probability of first hitting the set B at the point y when starting point $x\notin B$. If the set $B\in\mathbb{Z}_2$ consists of at least two points, then the following formula holds:

$$H_B(x,y)=\frac{K_B(y)}{K_B}-\sum_{t\in B}A(x,t)\left[K_B(t,y)-\frac{K_B(t)K_B(y)}{K_B}\right]. \tag{12}$$

In the diffusion-limited aggregation it is assumed that the particle starts from infinity: $|x|\to\infty$. For such a case it can be shown that the formula (12) reduces to a simpler expression (Ref. 29, theorem 14.1):

$$H_B(\infty,y)\equiv p_B(y)=\frac{K_B(y)}{K_B}. \tag{13}$$

This function $p_B(y)$ provides the so-called harmonic measure of the set B: $\sum_y p_B(y)=1$.

Now the prescription for how to calculate efficiently the potential kernel (9) is needed. First of all, due to the translational symmetry of the simple random walk, we have

$$A(x,y)=a(x-y),$$

where the function $a(x)$ is given by the following integral:

$$a(x)=\frac{1}{(2\pi)^2}\int_{-\pi}^{\pi}\int_{\pi}^{\pi}\frac{1-\cos(m\theta_1+n\theta_2)}{1-\frac{1}{2}(\cos\theta_1+\cos\theta_2)}d\theta_1 d\theta_2. \tag{14}$$

Here the notation $x=(m,n)$ was introduced. The symmetry properties of the above integral show that

$$\begin{aligned}a(m,n)&=a(-m,-n)\\&=a(m,-n)\\&=a(-m,n)\\&=a(-n,m)\\&=a(n,-m)\\&=a,(n,m)\\&=a(-n,-m).\end{aligned} \tag{15}$$

The integral (14) can be calculated exactly only for points lying on the "diagonal" $x=(n,n)$; it can be shown that (Ref. 29, p. 149)

$$a(n,n)=\frac{4}{\pi}\sum_{k=1}^{n}\frac{1}{2k-1},\quad a(0,0)=0. \tag{16}$$

Because the double integral (14) cannot be calculated in the closed form for the points outside the diagonal, the following method of determination of $a(x)$ for arbitrary x is used. From the definition (8) the recurrence relation can be shown to hold:

$$4a(m,n)=a(n-1,m)+a(n+1,m)+a(n,m-1)+a(n,m+1). \tag{17}$$

By proper use of (15) and (17), the values (16) suffice to calculate the values of $a(x)$ for arbitrary x. Suppose the values of $a(k,m)$ for $0\le m\le k\le n$ are known. Then one can get $a(n+1,n)$ since $a(n,n)$ is the average of $a(n+1,n)$, $a(n-1,n)$, $a(n,n+1)$, and $a(n,n-1)=a(n,n+1)$. Next, $a(n+1,n+1)$ is found, the site $(n+1,n+1)$ being the only neighbor of $(n,n+1)$ where the value of $a(x)$ is unknown. In this way the values of $a(x)$ in the $(n+1)$st "column" can be determined, and then with the help of (15) the values of $a(x)$ for the remaining edges of the square can be obtained.

For large x it can be shown that

$$a(x)=\frac{1}{\pi}\{2\gamma+\ln[8(m^2+n^2)]\}, \tag{18}$$

where $\gamma=0.5772\ldots$ is the Euler constant. It should be stressed, however, that although in the neighborhood of the origin, the above formula is remarkably good, for the exact calculation of the extremely small hitting probabilities the indirect calculation of $a(x)$, as outlined above, is necessary. From formulas (6)–(14) we see that indeed the moments and $f(\alpha)$ are in fact expressed only in terms of coordinates of the aggregated particles.

III. THE IMPLEMENTATION

I have written a program for the generation of the DLA aggregates without simulating the random walks of the particles. As usual, at the beginning there was a single point (seed) with the perimeter consisting of the four sites. One of these sites was chosen with a probability $\frac{1}{4}$. Now the set B consisting of the points belonging to the perimeter was created. For this perimeter the computer calculated the matrix $A(x,y)$ and next the inverse matrix K_B was determined. My impression is that the matrix $A(x,y)$ is numerically well conditioned and there is no problem with inversion of it. I have found that the iterative scheme for the calculation of $a(x)$ described in Sec. II is *numerically unstable* and the largest available precision should be used to get the certain values of $a(x)$ on a lattice sufficiently large to embed the whole cluster. Then, according to formula (13), the probability of the hitting of the walker was ascribed to the points on the perimeter. With this probability distribution one of the points was chosen and added to the aggregate and the whole procedure was repeated. In previous simulations the particles started from the circle and some other methods were used to speed up the simulation, or the boundary condition for the Laplace equation was imposed on the finite square and the formula (13) *automatically* gives the probabilities for the walkers arriving from the *infinity*. Furthermore, we have at our disposal the probabilities of all points belonging to the perimeter with practically *arbitrary accuracy*.

I had performed two runs. In the first one I generated 270 DLA clusters consisting of up to $P=120$ (which corresponds to about 100 particles in the cluster) using the single precision to test some static characteristics like D and γ (see below). In the second run 400 DLA clusters were generated consisting of up to $P=79$ (N was of the order 60–65) and the calculations were done in the highest precision to measure accurately the small proba-

bilities and to perform the multifractal analysis. Because of the high accuracy of this method, I had no problem with discrimination between the completely screened sites and the sites with small p_s. The minimal probabilities were of the order 10^{-7} and for the screened sites, instead of zero, s have obtained sometimes $p_s \sim 10^{-19}$ (see Table II). Because of this large gap, there was no need to use the "burning" algorithm (one in which sites are successively labeled, or "burned," as in a forest fire) algorithm to identify the no-growth sites, as in Ref. 25.

IV. THE STATIC CHARACTERISTICS

In my approach the natural parameter characterizing the growth of the clusters is the number of P of sites on the perimeter, instead of the linear sizes R, or the number N of particles aggregated. It turns out that these three characteristic parameters are equivalent to each other: The number P is connected with the number of particles N by the relation of the form

$$P \sim N^{\gamma} , \tag{19}$$

with $\gamma = 0.92$ (see Fig. 1), and N is related to R via (1).

In Fig. 2 the plot of $\ln(N)$ versus $\ln(R)$ averaged over 270 clusters is shown; the straight part of the curve provides a check of the scaling formula (1). Unfortunately, the sample is too small to get a reliable value of the fractal dimension D. The slowing down of the curve for large R is natural and is caused by stopping of the growth process. During further growth the outer part of the cluster will attract new particles and this active zone moves outward and leaves behind a frozen structure for which the plot $\ln N$ versus $\ln R$ will have the slope D. It turns out that the scaling properties of the DLA fractals can be expressed in a slightly different way. Namely, let $\langle R_N \rangle$ denote the average distance of the Nth particle from the center:

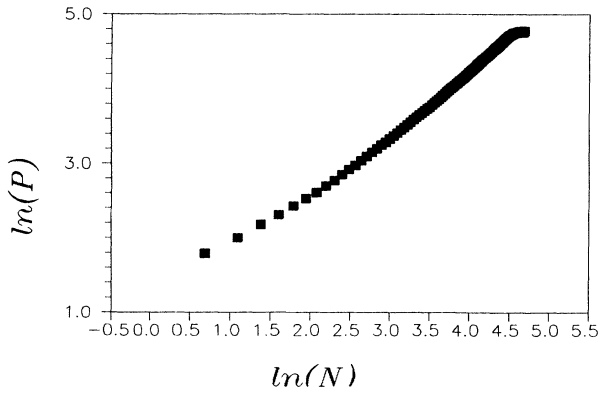

FIG. 1. The plot of $\ln(P)$ vs $\ln(N)$ averaged over 270 aggregates. The equation of the straight line has the form $\ln(P) = 0.58 + 0.92 \ln(N)$. The fact that these points lie on a straight line allows us to use the number of sites in the perimeter instead of the number of particles or the size of the aggregate.

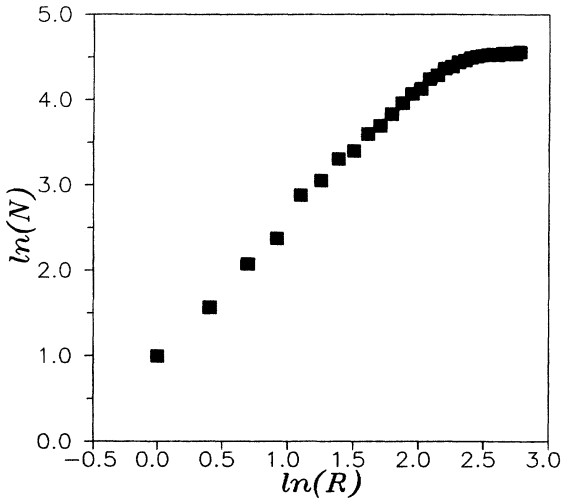

FIG. 2. The plot of $\ln(N)$ vs $\ln(R)$. The value of the number $N(R)$ of particles inside the circle of radius R was averaged over all clusters.

$$\langle R_N \rangle = \frac{1}{N_{\rm cl}} \sum_{i=1}^{N_{\rm cl}} R_N^{(i)} , \tag{20}$$

where $N_{\rm cl}$ is the number of clusters and $R_N^{(i)}$ is the distance from the center of the Nth particle belonging to the ith cluster. In Fig. 3 the plot of $\ln(\langle R_N \rangle)$ versus $\ln(N)$ is shown; this curve contains 112 points in contrast to Fig. 2, where the number of points is 31. The very long straight-line part enables quite accurate determination of the slope, which turns out to be equal to $0.582 = 1/1.72 = 1/D$. This fact leads to the conjecture

$$\langle R_N \rangle \sim N^{1/D} . \tag{21}$$

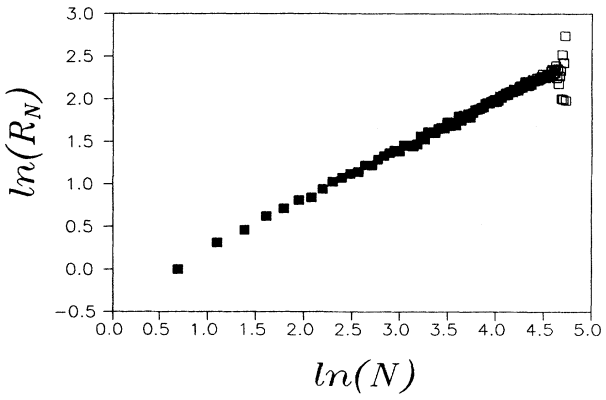

FIG. 3. The plot of $\ln\langle R_N \rangle$ vs N. The solid boxes denote the points averaged over all 270 clusters and the empty boxes represent fluctuation resulting from averaging over less than 270 clusters. The equation of the straight line (fitted only to the solid boxes) is $\ln\langle R_N \rangle = -0.34 + 0.582 \ln N$, with the variance 4.5×10^{-4}.

I would like to stress that the equivalence of (1) and (21) is not obvious, since the Nth particle will usually be hit in the shell of a finite width and the R_N will be less than the actual radius of the cluster.

V. THE "GLOBAL" MULTIFRACTALITY

From the above discussion the fundamental role of the set of hitting probabilities $\{p_s\}$ for the theoretical description of the growth process is evident. The customary tool for description of the set of probabilities is the family of the moments[30] defined in Eq. (2). These moments are averaged over the sample of the clusters—e.g., in Ref. 16 the moments were averaged over 1000 clusters consisting of 100 particles and in Refs. 23 and 25 the averaging was done over *all* configurations but in a small lattice of the size 5×5. Using my method, where the natural parameter describing the process of the growth is the number P of sites on the perimeter, it is natural to define the moments in the following way:

$$Z_q(P)=\frac{1}{N_{\rm cl}}\sum_{i=1}^{N_{\rm cl}}\sum_{s=1}^{P}(p_s^{(i)})^q\ , \tag{22}$$

where $p_s^{(i)}$ is the probability of the sth perimeter site in the ith cluster. The dependence of the moments on P is explicit in the upper limit of the inner sum and is implicit in $p_s^{(i)}$. In the orthodox approach,[15–19] which I will call the "global" multifractality, these moments should depend on P in the powerlike manner:

$$Z_q(P)=A(q)P^{-\tau(q)}\ . \tag{23}$$

The function $\tau(q)$ is global in the sense that it is independent of P (in the limit $P\to\infty$) if scaling is fulfilled exactly. I have generated 400 DLA clusters consisting of up to $P=79$ that corresponds to about 60–65 particles in the aggregate. At five stages of the growth process ($P=59$–60, 64–65, ..., 78–79) the actual $p_s^{(i)}$ were recorded. (The size of the perimeter can change also by two sites.)

In Fig. 4 a sample of the plots of $\ln[Z_q(P)]$ versus $\ln(P)$ for different q's is shown. As expected, for positive q the data points form perfect straight lines, which confirms the power-law dependence of $Z_q(P)$. For negative q's the plots do not have a constant slope [equal to $\tau(q)$] and the curves seem to be exponentially increasing. The more evident exponential increase of the moments with the logarithm of the lattice size was observed in Refs. 23 and 25. These authors averaged moments over *all* clusters and they include into the moments also the absolutely small probabilities appearing in the very little clusters but giving the dominant contribution for the negative q. Because of the small number of clusters used for the averaging, the increase of $\ln[Z_q(P)]$ is slower than that reported in Refs. 23 and 25. I would like to refer to Fig. 3 in Ref. 31 where the example of the plot of $\ln Z_q(P)$ versus $\ln L$ is presented for the real fluid experiment and the scaling is also not quite clear.

Another way of testing whether the scaling law (23) is fulfilled or not is the calculation of the prefactor $A(q)$ for each P separately with $\tau(q)$ determined "globally." If the scaling were fulfilled, then all functions $A(q,P)$ would coincide. In Fig. 5 the plots of $\ln A(q,P)$ are shown and, indeed, there is a large scaling regime and only for sufficiently negative q do small splittings appear. This *slight* deviation from the scaling is obviously due to the averaging of the moments only over the *typical aggregates.*

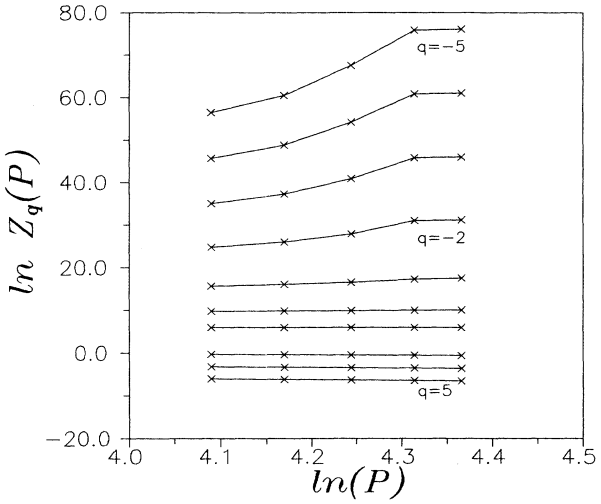

FIG. 4. The plots of $\ln Z_q(P)$ vs $\ln(P)$ for $q=-5$–5 with the exception of $q=1$ [by definition $Z_1(P)=1$].

Although it is not clear whether the scaling is fulfilled for negative q or not, the function $\tau(q)$ was determined

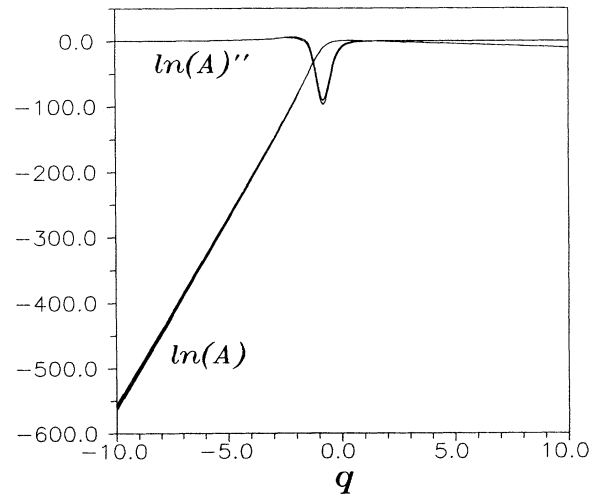

FIG. 5. The plot of the $\ln A(q,P)$ for five values of P. The small splitting of these curves for large negative q is the evidence for the breakdown of the scaling law. The second derivative of it and of the difference $\ln A(q,P)-\ln Z_q(P)$ is also shown; as these latter two curves almost coincide, there is a small influence coming from the moments $Z_q(P)$.

for all q by fitting the straight lines to the points ($\ln P$, $\ln Z_q(P)$). The plot of the "global" $f(\alpha)$, being the Legendre transform of $\tau(q)$ defined in (4), is shown in Fig. 6. For $\alpha \approx 18.5$ there is a cusp and the function $f(\alpha)$ is nonanalytical there. This cusp is caused by the turnback of $\alpha(q)$ for $q \approx -1.5$ (see Fig. 7). This nonmonotonicity of $\alpha(q)$ is in contradiction with the general properties of this function. The explanation for the nonmonotonicity of $\alpha(q)$ can be twofold. Apart from the scaling violation, another reason for the cusp can be a bad behavior of the prefactor $A(q)$ in conjunction with the small values of P. Indeed, from (23) it follows that

$$\tau(q)=\frac{\ln A(q)}{\ln P}-\frac{\ln Z_q(P)}{\ln P} . \tag{24}$$

Although the second derivative of $\ln Z_q(P)$ is positive (see the Appendix):

$$\frac{d}{dq}\ln Z_q(P)\geq 0 , \tag{25}$$

it is insufficient to ensure that $\alpha(q)$ is monotonically decreasing because for *finite* P the prefactor $A(q)$ can give the contribution of the opposite sign—only in the thermodynamic limit $P\rightarrow\infty$ do we obtain that $\alpha'(q)<0$. In Fig. 5 the plot of the second derivative of $\ln A(q)$ is also shown and there is an interval where it is indeed positive. The difference of the second derivatives of $\ln Z(P)$ and $\ln A(q)$ is also shown in this figure. Because

$$[\ln A(q)-\ln Z_q(P)]''>0, \quad \text{for } q\approx -1.5 \tag{26}$$

it follows that the cusp is not due to the breaking of the scaling law but the nonmonotonicity of $\alpha(q)$ is caused by the bad behavior of the prefactor $A(q)$. In the thermodynamic limit the influence of $A(q)$ would probably be negligible and the cusp should disappear.[32] Of course, there is some contribution coming from the fitting by least-squares method of straight lines to the points ($\ln Z_q$, $\ln P$). Those points, in fact, do not lie on the straight lines but this is insufficient as an explanation of the cusp in the plot of $f(\alpha)$. To show it, I have used for the least-squares determination of $\tau(q)$ only *two* arbitrary points ($\ln Z_q(P)$, $\ln P$) which obviously lie on the straight line and the cusp was still present in the plot of $f(\alpha)$.

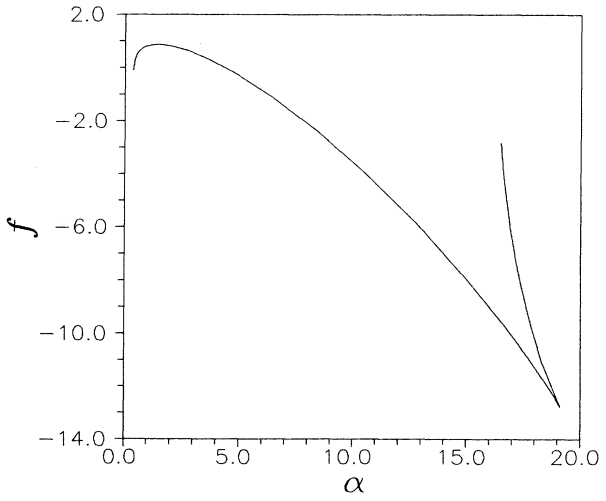

FIG. 6. The function $f(\alpha)$ obtained by least-squares fitting. The unusual values of α and f are caused by the fact that the scaling of the moments with respect to the number of perimeter sites is used.

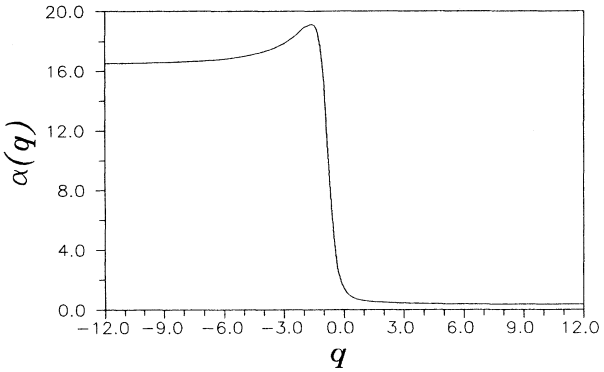

FIG. 7. The plot of the function $\alpha(q)$. This function is not monotonically decreasing—it has the local maximum at $q\approx -1.5$. The abrupt increase begins at $q_c=0$. As the jump appears in the narrow region, it indeed resembles the phase transition.

VI. THE "LOCAL" MULTIFRACTALITY

In this section I will discuss the "local" functions $\tau(q,P)$, $\alpha(q,P)$ and $f(\alpha,P)$ defined in Refs. 23–26 as

$$\tau(q,P)\equiv -\ln Z_q(P)/\ln P , \tag{27}$$

$$\alpha(q,P)\equiv\frac{d\tau(q,P)}{dq} ,$$
$$f(\alpha,P)\equiv q\alpha(q,P)-\tau(q,P) . \tag{28}$$

In Fig. 8 the functions $f(q,P)$ are plotted. The values taken by f's (and other functions plotted on the following figures) are rather unusual. This is caused by looking for the scaling of the moments with respect to the number of perimeter sites P and not N or R. However, in view of the scaling relations (1) and (19), these two quantities are equivalent and the functions $\tau(q,R)$, $\alpha(q,R)$, and $f(q,R)$ are related to the functions (27) and (28) by means of the rescalings

$$\phi(q,R)=\gamma D\phi(q,P), \quad \phi=\tau,\alpha,f . \tag{29}$$

The values of $f(q,P)$ are also smaller than the values of the "global" $f(\alpha)$ due to the factor $\ln P$ [see (27)]. The negative values of $f(\alpha)$ are connected with the nongeometrical character of the measure; see also Ref. 33 where the negative $f(\alpha)$ were found for the self-similar resistor networks. Recently, the significance of the negative $f(\alpha)$'s was stressed by Mandelbrot (see Ref. 34).

The plots presented in Fig. 8(a) suggest that because the slopes on both sides of $q_c=0$ are different, there can be a first-order phase transition. This kind of phase transition was suspected by Blumenfeld and Aharony[24] and

the value of q_c agrees with the one predicted by them. It follows that $q_c(P)$ does not depend on P, as observed in Ref. 23 and predicted by BA for the thermodynamic limit, [see Fig. 8(b)]. The shapes of $f(q,P)$ suggest that in the thermodynamic limit $P\to\infty$, the function $f(q,\infty)$ can become discontinuous at $q_c=0$ [see Fig. 8(c)]. In such a case the phase transition would be better called "zeroth order."

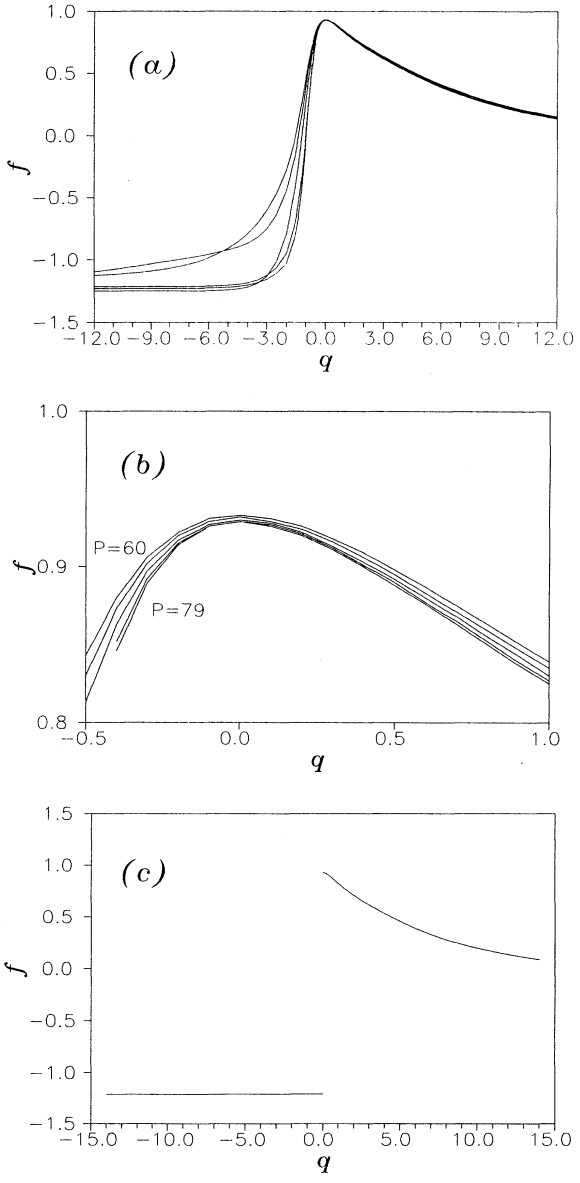

FIG. 8. The dependence of $f(q,P)$ on q. The negative values of f are possible since the measure is probabilistic and not a geometrical one. Exactly at $q_c=0$, all f's have the first derivative equal to zero (b) and on both sides of this point derivatives are of opposite sign. For larger P (thermodynamic limit) plots on the left of $q_c=0.0$ are becoming sharper and for $P\to\infty$, $f(q,P)$ can become discontinuous at $q_c=0$ [see (c)].

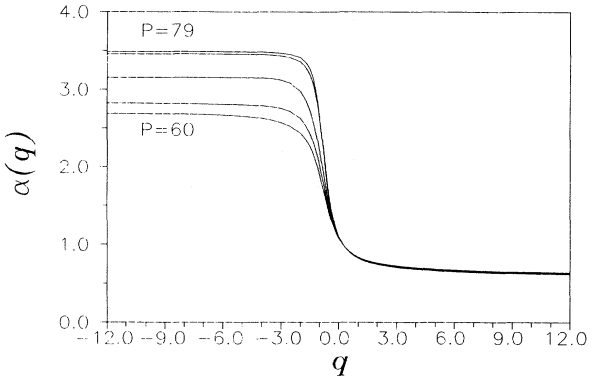

FIG. 9. The plots of $\alpha(q,P)$.

The plots of $\alpha(q,P)$ are reproduced in Fig. 9 and they are quite similar to the ones depicted in Fig. 1(b) of Ref. 24; there is a slow decreasing of $\alpha_{\min}(P)$ with P from 0.63 for $P=60$ to 0.61 for $P=79$ and larger increasing of $\alpha_{\max}(P)$ from 2.7 to 3.5 with P. Let us note that $\alpha(q,P)$ quickly become flat for $q<q_c$ and for $q>q_c$ they are slowly converging to the asymptotic values $\alpha_{\min}(P)$. Finally, in Fig. 10 the functions $f(\alpha,P)$ are shown. The negative values of $f(\alpha)$ are the consequence of the nongeometrical character of the measure appearing in (22) (see Refs. 33 and 34).

Besides q_c BA introduced in Ref. 24 a second threshold denoted by q_0, such that for $q<q_0$ the functions α and f are constant. Both the functions $f(q)$ and $\alpha(q)$ suggest that $q_0(P)$ tends to 0 with increasing P, as suspected by BA.

In previous papers[23–26] the splitting of the curves $f(q,P)$ for $q<q_c$ (Fig. 8) was linked to the violation of the scaling law and it was treated as the signal of the phase transition at q_c. I would like to point out another

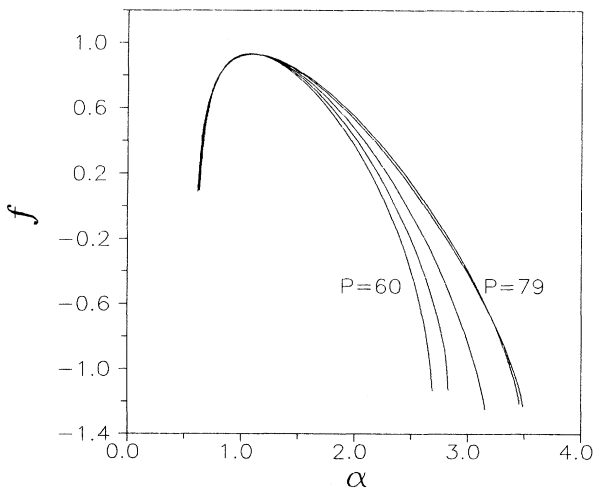

FIG. 10. The f's plotted as functions of α. This figure should be compared with Fig. 12 in Ref. 26.

TABLE I. The difference between consecutive $\alpha(\pm\infty,P)$ compared with the values predicted by Eq. (32).

P	$a_{\max}(P+5)-\alpha_{\max}(P)$	Eq. (32)	$\alpha_{\min}(P+5)-\alpha_{\min}(P)$	Eq. (32)
60	0.1364	0.2710	−0.0044	−0.0054
65	0.3331	0.2419	−0.0047	−0.0049
70	0.3334	0.2170	−0.0050	−0.0044
75	−0.0311	0.1601	−0.0037	−0.0032

possible reason for these splittings: for small P the prefactor $A(q)$ in the definition (28) can be relevant. For finite P the function $\tau(q)$ obtained by means of this prescription differs from the critical exponents appearing in (23). In previous Sec. V I have shown that this prefactor is also responsible for the cusp in the plot of the global $f(\alpha)$ in Fig. 6. The phase transition appears at $q_c=0$ and the cusp is connected with the local maximum of the global $\alpha(q)$ for $q\cong -1.5\neq q_c$.

The "global" functions $\tau(q),\alpha(q),f(q)$ were determined by the least-squares method and they automatically are accounted for the prefactor. These functions are related to the local functions defined by (27) and (28) by the following formulas:

$$\alpha(q)=\alpha(q,P)+\frac{1}{\ln P}\frac{d}{dq}\ln A(q)\ , \tag{30a}$$

$$f(\alpha)=f(\alpha,P)+\frac{qd\ln A(q)/dq-ln\,A(q)}{\ln P}\ . \tag{30b}$$

From Fig. 5 it follows that for sufficiently large $|q|$ the function $\ln A(q)$ is linear:

$$\ln A(q)=a_{\pm}q+b_{\pm}\ , \tag{31}$$

with $a_+=-1.15$, $b_+=1.32$, and $a_-=57.5$, $b_-=14.7$, appropriately for $q>>0$ and $q<<0$. The splitting between two consecutive $\alpha_{\min,\max}(P)$ is given by

$$\alpha_{\min,\max}(P+5)-\alpha_{\min,\max}(P)=a_{\pm}\left[\frac{1}{\ln(P)}-\frac{1}{\ln(P+5)}\right] \tag{32}$$

and the splitting between the appropriate limiting values of $f(q,P)$'s is given by the similar formula with $a_{\pm}$ replaced by $b_{\pm}$. In Table I the comparison of formula (32) with real values of the splittings is presented. The agreement is better for positive q's where there is no violation of the scaling law; nevertheless, for negative q's at least a part of the splittings can be linked to the prefactor. If there is indeed a phase transition to a non-power-law form for $p_{\min}$, which cannot be excluded by my data (see Sec. VII and Fig. 11), then splittings are not due to the prefactor, but are inherent. Because the value of b_- is smaller then a_-, the splittings between $f_{-\infty}(P)$'s are smaller than those between $\alpha_{\max}(P)$'s.

The analysis given in Ref. 24 was based on the assumption that the number of sites having a minimal growth probability $n(p_{\min})$ increased with P like $n(p_{\min})\sim P^{d_{\min}}$ and BA derived the relation $d_{\min}=f(-\infty)$. I cannot unfortunately confirm the existence of such an index $d_{\min}=f(-\infty)$. I have found that $d_{\min}$ varies very strongly with the size of the bins used for determination of $n(p)$. Besides, the $f(-\infty)$ is negative and $d_{\min}$ obviously should be positive.

VII. PHASE TRANSITION AND THE MINIMUM GROWTH PROBABILITIES

The breakdown of the scaling law (23) was attributed (in Refs. 23 and 24) to the existence of the sites on the perimeter of DLA clusters with extremely small hitting probabilities. These small probabilities give the dominant contribution to the moments for negative q and it was called the "negative-moment problem." In previous works (see Sec. VIII) no reliable information on probabilities in the "fjords" of the DLA clusters was obtained. Blumenfeld and Aharony assumed in Ref. 24 that the minimal probabilities $p_{\min}$ decrease exponentially with the size L of the growing aggregates:

$$p_{\min}(L)\sim\exp(-A_1L^x)\ , \tag{33}$$

with A_1 and x size independent. The data obtained by means of the method described in Sec. II allow in principle the checking of the assumption (33). It is reasonable to define the minimum hitting probability of a *typical* cluster as the average

$$p_{\min}(P)=\frac{1}{N_{\rm cl}}\sum_{i=1}^{N_{\rm cl}}p_{\min}^{(i)}(P)\ , \tag{34}$$

where $p_{\min}^{(i)}(P)$ is the minimal probability of the ith cluster with the perimeter consisting of P sites. In Fig. 11 the plot of $\ln p_{\min}(P)$ versus P is shown. The points lie almost exactly on the straight line and

$$p_{\min}(P)\sim\exp(-A_1'P),\quad A_1'=0.044\ . \tag{35a}$$

Unfortunately, the restriction to small cluster sizes (limited by the computer's capabilities) does not allow ruling out the possible powerlike decay of $p_{\min}$, [see Fig. 11(a)]. Here the points follow the power law

$$p_{\min}\sim P^B,\quad B=3.0\ . \tag{35b}$$

To discriminate between these two possible laws, the gaps between consecutive P's, at which growth probabilities are recorded, should increase in exponential way. Recently (Ref. 35), yet another form of the behavior of $p_{\min}$ was anticipated:

$$\ln p_{\min}(N)\sim-(\ln N)^y,\quad y\cong 2 \tag{35c}$$

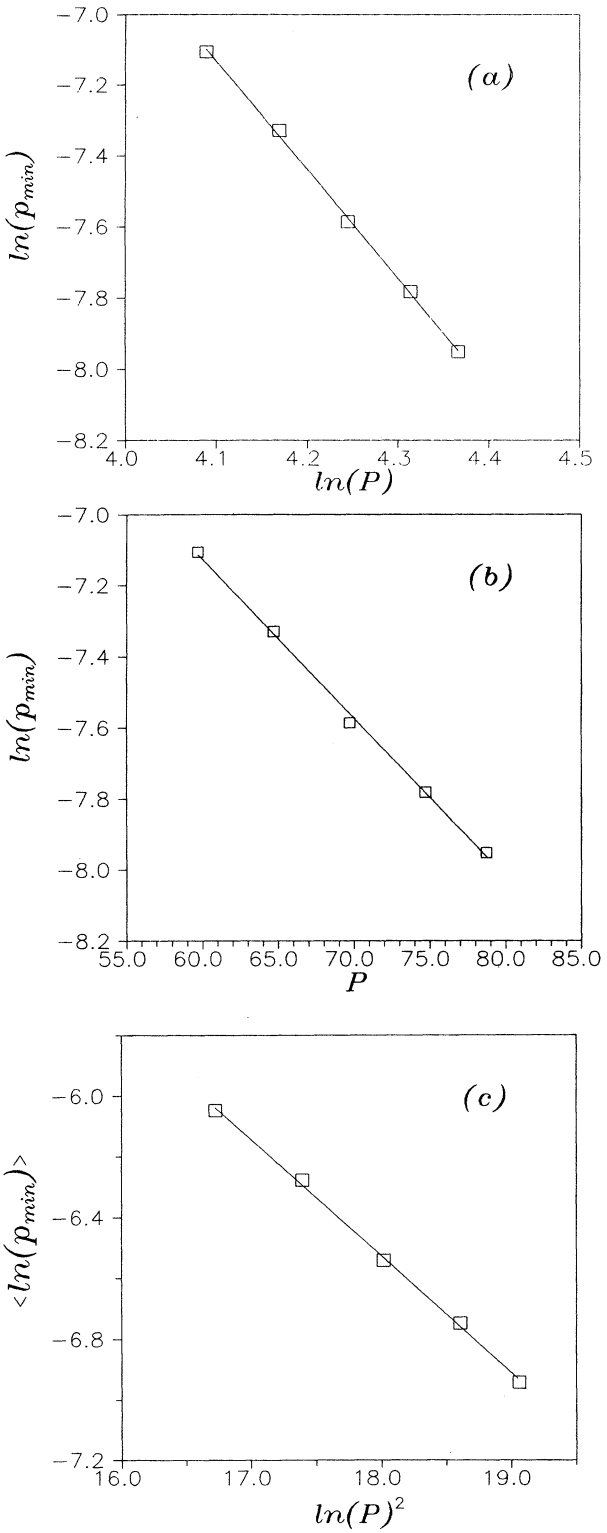

FIG. 11. The dependence of the typical minimum growth probability on P: In (a) the plot of $\ln p_{\min}$ vs $\ln P$ is shown, in (b) the plot of $\ln p_{\min}$ vs P is shown, and in (c) the average over 400 clusters of $\ln p_{\min}$ vs $\ln(P)^2$ is plotted. The sizes of the clusters are too small to allow the discrimination between these three possible dependences. The abscissas are the mean values of numbers of the perimeter sites among 400 clusters.

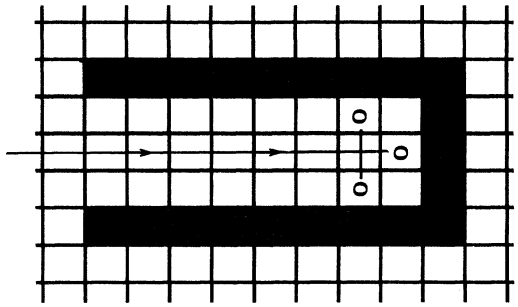

FIG. 12. The three perimeter nodes denoted by circles have the lowest probability among the clusters of N particles—to reach these sites, the walker has to follow a straight line. For these configurations $P=2N$ and above $N=21$ and $P=42$.

[see also Fig. 11(c) where the average over 400 clusters of $\ln p_{\min}$ versus $\ln(P)^2$ is plotted]. The fact that P appears in (35) in the power 1 suggests that P is a natural parameter describing the growth process. The small value of the factor A_1' suggests that the possible breakdown of the scaling is not big (compare Fig. 5), as conjectured in Ref. 28. It should be stressed that the rate of decrease (35) is almost an order of magnitude smaller than that for the *absolute* minimal growth probability of the cluster consisting of N particles. These absolute minimal probabilities p_{MIN} (please notice the difference in notation—now there are capital letters MIN) are linked to the nodes that can be reached only along *one* way of the largest possible length at the fixed number of perimeter sites. Configurations possessing such a property are simply the tunnel-like clusters[26,28] (see Fig. 12). I have generated a series of such tunnel-like clusters and calculated the hitting probabilities. It turns out that the smallest probability decreases with P $(=2N)$ *exactly* according to $p_{\mathrm{MIN}}(P) \sim \exp(-AP)$, with $A=0.334$ (see Fig. 13). A

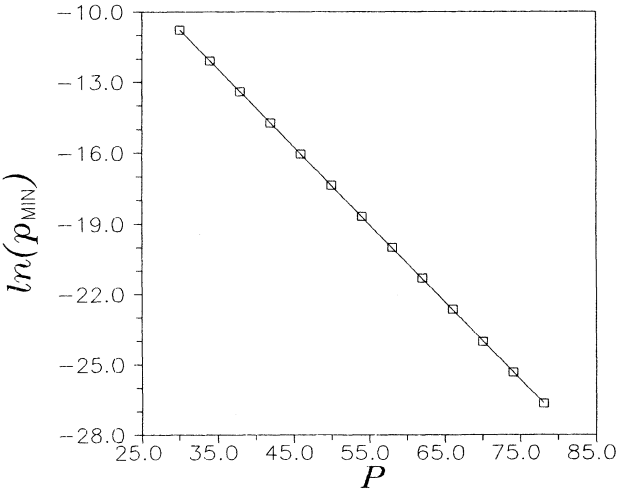

FIG. 13. The plot of $\ln p_{\mathrm{MIN}}(P)$ vs P for the nodes marked in Fig. 12 by circles for $P=30,34,\ldots,78$.

simple heuristic argument shows that $A=(\ln 4)/4 \approx 0.346$. Indeed, to reach one of the three sites deeply inside the tunnel, the walker has to follow only one way of the length $L=(P-10)/4$ and $p_{\min}=p^*(\frac{1}{4})^L$, where p^* denotes the probability of hitting the entrance to the tunnel. Assuming the weak dependence of p^* on P, it follows that

$$p_{\min}(P) \sim \exp[-\ln(4)/4P] \ . \tag{36}$$

Because in Refs. 23 and 25 the averaging was over *all* configurations, such rare tunnel-like clusters were therefore also included into the moments and they are responsible for the much larger breakdown of the scaling reported in those papers.

The values of $p_{\min}(P)$ calculated according to (34) are in some sense misleading due to the large fluctuations: The absolute minimum growth probability among the 400 clusters was 2.96×10^{-7}, and the largest $p_{\min}^{(i)}$ was 4.11×10^{-3} (see Fig. 14). In Fig. 15 the plot of $n(p_{\min})$ is given, where the quantity $n(p_{\min})$ is defined by $n(p_{\min})$ being the number of clusters with growth probabilities in the range $\ln p_{\min}\pm\Delta/2$ with $\Delta=0.2$. In my opinion these large fluctuations of the $p_{\min}^{(i)}$ are also contribution to the violation of the scaling law (23). To justify this statement, I would like to discuss the $q\gg0$ limit of the multifractal spectrum. For positive q's the contribution from the maximum growth probabilities dominates the moments $Z_q(P)$:

$$Z_q(P)=\frac{1}{N_{\rm cl}}\sum_{i=1}^{N_{\rm cl}}(p_{\max}^{(i)})^q, \quad \text{for } q\gg0 \tag{37}$$

where $p_{\max}^{(i)}$ denotes the largest hitting probabilities on the perimeter of the ith cluster. In Refs. 14 and 17 the powerlike decrease of $p_{\max}$ was observed. Defining the typical $p_{\max}$ as the average

$$p_{\max}=\frac{1}{N_{\rm cl}}\sum_{i=1}^{N_{\rm cl}}p_{\max}^{(i)} \ , \tag{38}$$

I have found from my data the following dependence:

$$p_{\max}=aP^{-b}, \quad a=-1.18, \quad b=0.35 \tag{39}$$

(see Fig. 16). In order to get from (37)–(39) a conclusion about the scaling of the moments, one should be able to interchange the averaging with rising to the qth power. The equality

$$\frac{1}{n}\sum_{i=1}^{n}a_i^q=\left[\frac{1}{n}\sum_{i=1}^{n}a_i\right]^q \tag{40}$$

holds only when all terms are equal: $a_1=a_j$, $i,j=1,\ldots,n$. It turns out that indeed the values $p_{\max}^{(i)}$, $i=1,\ldots,400$, are almost equal: They are contained in the narrow interval $(4.5\times10^{-2},7.6\times10^{-2})$ and it seems to be obvious. It allows us to rewrite (37) as

$$Z_q(P)=a^qP^{-bq} \tag{41}$$

and it follows that $b=\alpha(\infty)$. This relation really holds with a great accuracy because $\alpha(\infty)=0.3553$, [see Fig. 7 and Eq. (39)]. From (41) it follows that $A(q)=a^q$ for

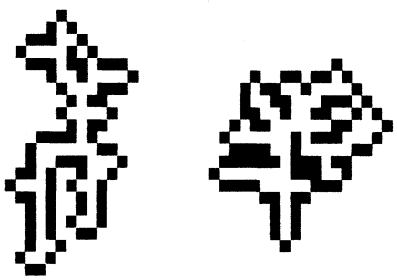

FIG. 14. Shapes of the perimeters containing nodes with the smallest $p_{\min}$ (left) and largest $p_{\min}$ (right).

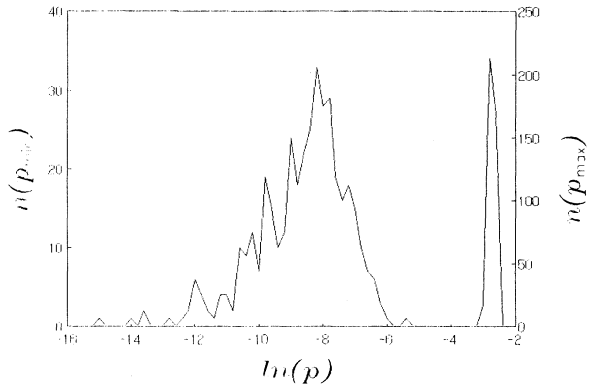

FIG. 15. The histogram showing the number of clusters with $P=78$ or 79 having $\ln p_{\min}$ contained in the interval of length 0.2 around $\ln p_{\min}$ ($\ln p_{\max}$ on the left side). The left scale is for $n(\ln p_{\max})$.

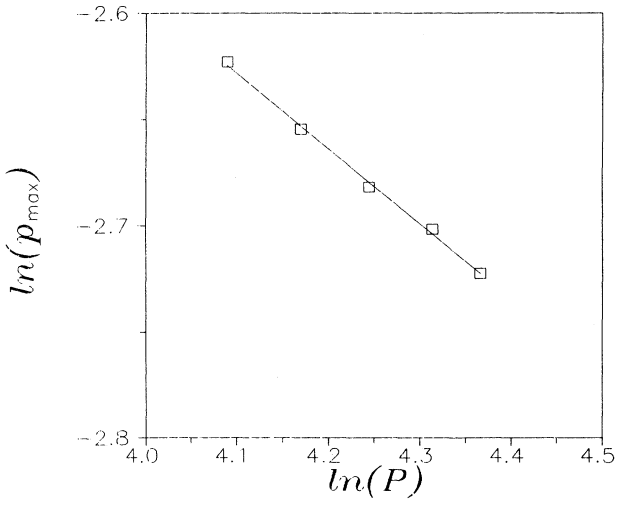

FIG. 16. The plot of the $\ln p_{\max}$ vs $\ln P$ averaged over 400 clusters. The points follow the straight line $\ln p_{\max}=-1.18-0.353\ln P$ with the variance 3×10^{-6}.

TABLE II. Values of p_s for the perimeter sites of the cluster shown in Fig. 17. In column 2 the probabilities obtained via Spitzer's theorem are given. Columns 3–5 provide the values obtained by means of solution of the Laplace equation on the lattices of sizes 71×71 and 121×121 with two different boundary conditions: 0 on the cluster and 1 on the boundary, and 1 on the cluster and 0 on the edges of the square. Column 6 shows the probabilities obtained by the Monte Carlo simulation with help of 100 000 random walkers. The asterisk denotes the completely screened sites for which $p_s=0$. $x[y[$ denotes $x\times10^{y}$.

Site number	Theorem of Spitzer	0.0 on DLA 71×71	1.0 on DLA 71×71	1.0 on DLA 121×121	Monte Carlo
1	4.3022[−2]	2.6023[−2]	3.7008[−2]	3.7106[−2]	4.5250[−2]
2	3.4976[−2]	2.3482[−2]	3.3305[−2]	3.3379[−2]	3.8540[−2]
3	3.5535[−2]	2.0617[−2]	2.9377[−2]	2.9463[−2]	3.7900[−2]
4	1.0710[−2]	1.0434[−2]	1.4623[−2]	1.4648[−2]	1.1980[−2]
5	2.4106[−2]	1.5420[−2]	2.1340[−2]	2.1373[−2]	2.4690[−2]
6	1.0596[−2]	1.1415[−2]	1.6270[−2]	1.6316[−2]	1.1050[−2]
7	1.3973[−2]	1.2040[−2]	1.4263[−2]	1.4281[−2]	1.5290[−2]
8	2.1432[−2]	1.6332[−2]	2.2439[−2]	2.2467[−2]	2.2580[−2]
9	2.9520[−2]	1.8481[−2]	2.5921[−2]	2.5952[−2]	3.0870[−2]
10	2.3304[−2]	1.5764[−2]	2.2480[−2]	2.2533[−2]	2.5520[−2]
11*	2.6613[−20]	−1.0771[−193]	0.0000	0.0000	0.0000
12	3.6072[−4]	3.8037[−3]	2.3174[−3]	2.3202[−3]	4.6000[−4]
13	6.5329[−3]	7.2219[−3]	8.0561[−3]	8.0667[−3]	6.5900[−3]
14	1.0680[−2]	1.0655[−2]	1.5100[−2]	1.5114[−2]	1.1520[−2]
15	3.1147[−2]	1.7923[−2]	2.5462[−2]	2.5480[−2]	3.1930[−2]
16	2.8503[−2]	1.8469[−2]	2.6341[−2]	2.6388[−2]	2.8910[−2]
17*	0.0000	9.1288[−3]	1.3019[−2]	1.3046[−2]	0.0000
18*	1.4016[−19]	2.2822[−3]	3.2547[−3]	3.2617[−3]	0.0000
19*	0.0000	−3.1170[−195]	0.0000	0.0000	0.0000
20	9.6622[−5]	5.3571[−3]	1.7171[−3]	1.7193[−3]	1.1000[−4]
21	1.4493[−3]	1.3617[−2]	3.8221[−3]	3.8272[−3]	1.3000[−3]
22	3.4083[−2]	1.8627[−2]	2.6525[−2]	2.6520[−2]	3.5600[−2]
23	5.9458[−2]	2.9406[−2]	4.1939[−2]	4.1976[−2]	6.3130[−2]
24	2.5766[−5]	5.8781[−3]	8.5375[−4]	8.5486[−4]	3.0000[−5]
25	6.4415[−6]	1.3455[−2]	4.8424[−4]	4.8493[−4]	1.0000[−5]
26*	0.0000	3.3065[−4]	4.7111[−4]	4.7065[−4]	0.0000
27*	1.7556[−20]	1.2399[−3]	1.7667[−3]	1.7651[−3]	0.0000
28	3.0809[−3]	4.6291[−3]	6.5956[−3]	6.5901[−3]	3.3400[−3]
29	1.3536[−2]	1.3340[−2]	1.9015[−2]	1.9025[−2]	1.4940[−2]
30*	2.0149[−19]	2.2369[−3]	3.1314[−3]	3.1331[−3]	0.0000
31	1.4330[−3]	2.7336[−3]	3.8011[−3]	3.8034[−3]	1.4800[−3]
32	1.0856[−3]	1.9724[−3]	2.7158[−3]	2.7175[−3]	8.3000[−4]
33	2.5766[−5]	2.4114[−2]	5.8190[−4]	5.8269[−4]	4.0000[−5]
34	6.4415[−6]	7.8300[−2]	6.2971[−4]	6.3059[−4]	0.0000
35*	1.7345[−19]	2.2939[−2]	2.7849[−4]	2.7889[−4]	0.0000
36*	0.0000	8.2663[−5]	1.1778[−4]	1.1769[−4]	0.0000
37*	3.4253[−19]	3.2891[−3]	4.6870[−3]	4.6823[−3]	0.0000
38	9.5011[−3]	8.5272[−3]	1.2153[−2]	1.2140[−2]	9.9500[−3]
39	3.4854[−2]	2.0710[−2]	2.9504[−2]	2.9520[−2]	3.6960[−2]
40	5.9144[−3]	6.2138[−3]	8.7244[−3]	8.7300[−3]	5.6600[−3]
41	1.0856[−3]	2.6105[−3]	3.4780[−3]	3.4806[−3]	1.1700[−3]
42	6.4202[−3]	8.2334[−3]	1.1739[−2]	1.1719[−2]	6.7600[−3]
43	2.6836[−2]	1.6101[−2]	2.2962[−2]	2.2915[−2]	2.5200[−2]
44	3.6083[−2]	1.9759[−2]	2.8040[−2]	2.8060[−2]	3.8140[−2]
45	5.0703[−3]	5.2862[−3]	6.8499[−3]	6.8555[−3]	5.2400[−3]
46*	0.0000	2.0368[−2]	3.6325[−4]	3.6356[−4]	0.0000
47*	3.1486[−2]	6.9340[−2]	1.8768[−4]	1.8784[−4]	0.0000
48*	0.0000	7.1775[−5]	1.0245[−4]	1.0221[−4]	0.0000
49*	2.4262[−21]	2.8710[−4]	4.0978[−4]	4.0889[−4]	0.0000
50*	2.1553[−20]	1.0766[−3]	1.5367[−3]	1.5335[−3]	0.0000
51*	0.0000	1.0740[−3]	1.5330[−3]	1.5299[−3]	0.0000
52	3.4124[−2]	2.0529[−2]	2.9289[−2]	2.9205[−2]	3.1860[−2]
53	2.1609[−3]	6.4355[−3]	4.3105[−3]	4.3144[−3]	2.3300[−3]
54*	0.0000	1.2132[−2]	1.2653[−3]	1.2665[−3]	0.0000
55*	2.4029[−20]	2.1726[−2]	3.8746[−4]	3.8784[−4]	0.0000

TABLE II. (*Continued*).

Site number	Theorem of Spitzer	0.0 or DLA 71×71	1.0 on DLA 71×71	1.0 on DLA 121×121	Monte Carlo
56	2.0602[−3]	2.9454[−3]	4.2040[−3]	4.1955[−3]	2.3500[−3]
57	2.4054[−3]	3.2195[−3]	4.5952[−3]	4.5863[−3]	2.3300[−3]
58*	0.0000	1.8681[−3]	2.6665[−3]	2.6616[−3]	0.0000
59	1.3915[−2]	1.3775[−2]	1.9655[−2]	1.9595[−2]	1.2950[−2]
60	2.7379[−3]	4.3910[−3]	4.7526[−3]	4.7571[−3]	2.8100[−3]
61*	0.0000	5.4315[−3]	9.6866[−5]	9.6959[−5]	0.0000
62*	0.0000	2.4696[−3]	3.5249[−3]	3.5177[−3]	0.0000
63	5.0118[−3]	4.8559[−3]	6.9308[−3]	6.9171[−3]	4.8500[−3]
64	1.0083[−2]	8.5939[−3]	1.2266[−2]	1.2244[−2]	8.5100[−3]
65	6.4635[−3]	7.4726[−3]	1.0666[−2]	1.0647[−2]	6.3100[−3]
66	6.5720[−2]	3.2986[−2]	4.7075[−2]	4.6940[−2]	5.9200[−2]
67	1.4044[−2]	1.2598[−2]	1.7498[−2]	1.7514[−2]	1.4820[−2]
68	2.9516[−3]	5.0226[−3]	7.1687[−3]	7.1547[−3]	2.8200[−3]
69	2.5685[−2]	2.0587[−2]	2.9384[−2]	2.9332[−2]	2.2830[−2]
70	4.3435[−2]	2.6880[−2]	3.8366[−2]	3.8288[−2]	3.8840[−2]
71	2.7745[−2]	1.6581[−2]	2.3427[−2]	2.3446[−2]	2.7420[−2]
72*	6.8518[−21]	−1.1845[−193]	0.0000	0.0000	0.0000
73	8.5113[−3]	8.1524[−3]	1.1636[−2]	1.1614[−2]	8.2500[−3]
74	2.4472[−2]	1.2745[−2]	1.8136[−2]	1.8142[−2]	2.4250[−2]
75	2.5406[−3]	3.2183[−3]	4.5933[−3]	4.5849[−3]	2.6500[−3]
76	2.7179[−2]	1.4352[−2]	2.0459[−2]	2.0452[−2]	2.6110[−2]
77	3.2361[−2]	1.8927[−2]	2.7012[−2]	2.6968[−2]	2.8630[−2]
78	4.1111[−2]	2.5522[−2]	3.6410[−2]	3.6371[−2]	3.8980[−2]
79	4.0835[−2]	2.5884[−2]	3.6934[−2]	3.6882[−2]	3.7930[−2]

large q and it also agrees with the numerical results: It is seen from Fig. 5 that $\ln A(q)$ is a linear function for positive q with the slope $a=-1.18$ [see (31)] and it agrees quite well with the value given in (39).

From this discussion it follows that even if the $p_{\min}$ would decrease in the powerlike way (which is not excluded by my data), the large fluctuation of $p_{\min}^{(i)}$ prevents the use of (40) leading to the scaling violation.

VIII. COMPARISON WITH OTHER METHODS

In this section I will present a comparison of the hitting probabilities for the one DLA cluster obtained by different methods. Three ways of calculation can be distinguished: the Monte Carlo method[15] using a large number of walkers probing the perimeter of the cluster, the analogy of DLA with the dielectric breakdown model,[8,19,22,27] and, recently, the approach based on the real-space renormalization-group arguments.[13]

The Monte Carlo estimation of the hitting probabilities is obtained by the successive launching of a large number (10^5-10^6) of random walkers and recording the first point of contact with the cluster. The advantage of this method is the possibility of treating the very large clusters (about 50 000 points), but the disadvantage is the poor values of the probability for deeply screened points. The dielectric breakdown model consists in the solution of the discretized Laplace equation. In this model the growth probability p_s at the growing perimeter site s is given by $p_s \sim (E_s)^\eta$, where E_s is the electric field at the site s and η is the parameter; for $\eta=1$ this model corresponds to the usual DLA.[8,19] The electric field is a gradient of the potential φ, which in turn satisfies the Laplace equation

$$\nabla^2\varphi=0 , \tag{42}$$

with the corresponding boundary condition. Two kinds of boundary conditions were used in the past: (a) with $\varphi=0$ on the cluster and 1 far away and (b) the opposite one: $\varphi=1$ on the cluster and 0 on the boundary of the lattice. For case (a) the field E_s is simply equal to the value of the potential while in case (b) $E_s=(\nabla\varphi)_s=1-\varphi_s$.

In Table II the hitting probabilities of the cluster shown in Fig. 17 obtained by means of the Spitzer theorem, the Laplace equation, and the Monte Carlo simulation are presented. The Laplace equation was solved by the relaxation method on the lattice 71×71 in the highest precision (19 to 20 digits) and on the lattice 121×121 with the single precision (6 to 7 digits). The calculation was continued until the *relative* error between two consecutive iterations was smaller than 10^{-10} at all sites and it needed over 1000 steps of the iteration. In the last column of Table II the probabilities obtained by Monte Carlo probing with 100 000 random walkers are given. The solution of the Laplace equation is over 10 times slower than the method based on the Spitzer theorem and launching of the 100 000 walkers needed 500 times more computer time.

For the region corresponding to the "tips" of the clus-

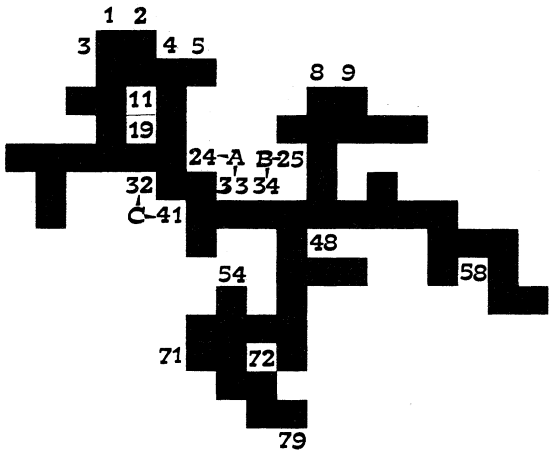

FIG. 17. The cluster consisting of the 65 particles with 79 sites on the perimeter. The perimeter sites are numerated from left to right in rows from the top to the bottom. The pairs of sites (24,33), (25,34), and (32,41) have the same p_s because they can be reached only from one common site denoted by A, B, and C, respectively.

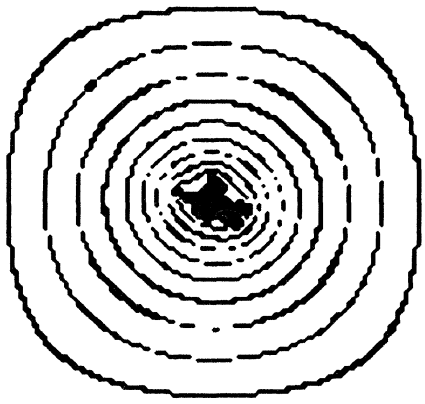

FIG. 18. The levels of equal values of solution of the Laplace equation with the boundary condition $\varphi=1.0$ on aggregate and on the lattice 121×121.

ters, where the hitting probabilities are highest, most of the methods seem to give similar results. Also, for the sites completely surrounded by particles of the aggregate (nodes 11, 19, 72), the solutions of the Laplace equation give zero. However, in the remaining screened sites (denoted in Table II by asterisks) the results obtained from the DBM analogy differ considerably from those obtained via the Spitzer theorem. Another check of accuracy of the methods is provided by the pairs of sites (25,34), (24,33), and (41,32) in Fig. 17, which by the symmetry arguments should have the same growth probabilities. In the first column all digits for the corresponding nodes coincide (in fact, the differences between p_s of sites belonging to these pairs were of the order 10^{-19}), and numbers in the next columns have no one common digit—only the orders coincide. The differences of the 2 to 3 orders also appear in other sites in "gulfs" and it puts into the question the $f(\alpha)$ spectrum obtained previously by solution of the Laplace equation (see Ref. 19). Solving the Laplace equation systematically gives larger values of p_c deeply in the "fjords," which may explain why the authors of Ref. 19 have not observed the phase transition.

The fact that all numbers in the third and fourth columns differ very little suggests that the effects caused by the finiteness of the lattice are in fact negligible—the size of the lattice has little influence upon the potential field near the cluster. Also, a rapid crossover from the square to the circular symmetry is visible in Fig. 18 where the levels of the equal values of φ are shown.

IX. CONCLUSIONS

The method of determination of the growth probabilities of DLA clusters based on the Spitzer theorem proposed in this paper seems to give more accurate results than previous ones. This method was used for the determination of the multifractal spectrum of DLA and I have found indications that at $q_c\cong0$ in the spectrum a phase transition appears. The discrimination between possible dependencies of minimum growth probabilities (35a)–(35c) can be done by means of the simulations of larger clusters.

ACKNOWLEDGMENT

This work was supported by the Research Project No. CPBP 01.02.

APPENDIX

From the definition (2) we get

$$\frac{d}{dq}\ln Z_q=\frac{1}{\chi_q}\sum_i p_i^q\ln p_i\le0\ ,$$

since $\ln p_i\le0$ for a probabilisitic measure. Therefore,

$$\frac{d^2}{dq^2}\ln Z_q=\bar{Z}_q^2\left[\sum_i p_i^q\sum_j p_j^q\ln p_j-\left[\sum_i p_i^q\ln p_i\right]^2\right]\ .$$

Now let us apply the Cauchy-Schwarz inequality,

$$\left[\sum_i a_ib_i\right]^2\le\sum_i a_i^2\sum_j b_j^2\ .$$

Putting here $a_i=p_i^{q/2}$, $b_i=p_i^{q/2}\ln p_i$, we obtain the desired result (25):

$$\frac{d^2}{dq^2}\ln Z_q\ge0\ .$$

This inequality means that $\tau(q)$ is convex in the *thermodynamic* limit and performing the Legendre transform is justified (see Ref. 36).

[1]T. A. Witten and L. M. Sander, Phys. Rev. Lett. **47**, 1400 (1981); Phys. Rev. B **27**, 5686 (1983).
[2]*On Growth and Form,* edited by H. E. Stanley and N. Ostrowsky (Nijhof, The Hague, 1985).
[3]H. J. Herrmann, Phys. Rep. **136**, 153 (1986).
[4]*Fractals in Physics,* edited by L. Pietronero and E. Tosatti (North-Holland, Amsterdam, 1986).
[5]H. E. Stanley, Philos. Mag. B **56**, 665 (1987).
[6]T. Vicsek, *Fractal Growth Phenomena* (World Scientific, Singapore, 1989).
[7]M. Matsushita, M. Sanyo, Y. Hayakawa, H. Honjo, and Y. Sawada, Phys. Rev. Lett. **53**, 286 (1984).
[8]L. Niemeyer, L. Pietronero, and H. J. Wiesmann, Phys. Rev. Lett. **52**, 1033 (1984).
[9]K. J. Måløy, J. Feder, and T. Jøssang, Phys. Rev. Lett. **55**, 2688 (1985).
[10]M. Muthukamar, Phys. Rev. Lett. **50**, 839 (1983).
[11]M. Tokuyama and K. Kawasaki, Phys. Lett. **100A**, 337 (1984).
[12]H. Gould, F. Family, and H. E. Stanley, Phys. Rev. Lett. **50**, 696 (1983); H. Nakanishi and F. Family, J. Phys. A **17**, 427 (1984); M. Kolb, *ibid.* **20**, L285 (1987).
[13]T. Nagatani, J. Phys. A **20**, L381 (1987); Phys. Rev. A **36**, 5812 (1987).
[14]L. Turkevich and H. Scher, Phys. Rev. Lett. **55**, 1026 (1985); and in *On Growth and Form* (Ref. 2), p. 293.
[15]P. Meakin, H. E. Stanley, A. Coniglio, and T. Witten, Phys. Rev. A **32**, 2364 (1985); T. C. Halsey, P. Meakin, and I. Procaccia, Phys. Rev. Lett. **56**, 854 (1986); P. Meakin, Phys. Rev. A **35**, 2234 (1987).
[16]C. Amitrano, A. Coniglio, and F. di Liberto, Phys. Rev. Lett. **57**, 1016 (1986).
[17]P. Meakin, A. Coniglio, H. E. Stanley, and T. A. Witten, Phys. Rev. A **34**, 3325 (1986).
[18]J. Nittmann, H. E. Stanley, E. Touboul, and G. Daccord, Phys. Rev. Lett. **58**, 619 (1987).
[19]Y. Hayakawa, S. Sato, and M. Matsushita, Phys. Rev. A **36**, 1963 (1987).
[20]R. Benzi, G. Paladin, G. Parisi, and A. Vulpiani, J. Phys. A **17**, 3521 (1984); T. C. Halsey, M. H. Jensen, L. P. Kadanoff, I. Procaccia, and B. Shraiman, Phys. Rev. A **33**, 1141 (1986).
[21]H. E. Stanley and P. Meakin, Nature **333**, 405 (1988).
[22]L. Pietronero, A. Erzan, and C. Evertsz, Physica A **151**, 207 1988.
[23]J. Lee and H. E. Stanley, Phys. Rev. Lett. **61**, 2945 (1988).
[24]R. Blumenfeld and A. Aharony, Phys. Rev. Lett. **62**, 2977 (1989).
[25]J. Lee, P. Alstrom, and H. E. Stanley, Phys. Rev. A **39**, 6545 (1989).
[26]J. Lee, P. Alstrom, and H. E. Stanley, Phys. Rev. Lett. **62**, 3013 (1989).
[27]S. Havlin, B. Trus, A. Bunde, and H. E. Roman, Phys. Rev. Lett. **63**, 1189 (1989).
[28]A. B. Harris, Phys. Rev. B **39**, 7292 (1989); A. B. Harris and M. Cohen, Phys. Rev. A **41**, 971 (1990).
[29]F. Spitzer, *Principles of the Random Walk* (Van Nostrand, Princeton, 1964), Theorem 12.1 p. 121, and Theorem 14.1 p. 141.
[30]A. Renyi, *Probability Theory* (North-Holland, Amsterdam, 1970).
[31]J. Nittmann, in *Universalities in Condensed Matter,* edited by R. Jullien *et al.* (Springer-Verlag, Berlin, 1989), p. 136.
[32]M. Wolf, J. Phys. A **22**, L1075 (1989); Physica A **160**, 24 (1989).
[33]B. Fourcade and A.-M.S. Tremblay, Phys. Rev. A **36**, 2352 (1987).
[34]B. Mandelbrot, in *Fractals,* edited by L. Pietronero (Plenum, New York, 1989); Physica A **163**, 306 (1990). I would like to thank A. Erzan for bringing these works to my attention.
[35]S. Schwarzer, J. Lee, A. Bunde, S. Havlin, H. E. Roman, and H. E. Stanley, Phys. Rev. Lett. **65**, 603 (1990).
[36]V. I. Arnold, *Mathematical Methods of Classical Mechanics* (Springer-Verlag, Berlin, 1978).